

**Geometric structure of anatase TiO<sub>2</sub>(101)**Jon P. W. Treacy,<sup>1</sup> Hadeel Hussain,<sup>1</sup> Xavier Torrelles,<sup>2</sup> David C. Grinter,<sup>3</sup> Gregory Cabailh,<sup>4</sup> Oier Bikondoa,<sup>5,6</sup> Christopher Nicklin,<sup>7</sup> Sencer Selcuk,<sup>8</sup> Annabella Selloni,<sup>8</sup> Robert Lindsay,<sup>1</sup> and Geoff Thornton<sup>3,\*</sup><sup>1</sup>*Corrosion and Protection Centre, School of Materials, The University of Manchester, Sackville Street, Manchester M13 9PL, United Kingdom*<sup>2</sup>*Institut de Ciència de Materials de Barcelona (CSIC), Campus UAB, 08193 Bellaterra, Spain*<sup>3</sup>*Department of Chemistry, London Centre for Nanotechnology, University College London, 20 Gordon Street, London WC1H 0AJ, United Kingdom*<sup>4</sup>*Institut des NanoSciences de Paris, Sorbonne Universités, UPMC Université Paris 06, CNRS-UMR 7588, F-75005 Paris, France*<sup>5</sup>*XMaS, The UK-CRG Beamline, ESRF, The European Synchrotron, 71 Avenue des Martyrs, F-38043 Grenoble, France*<sup>6</sup>*Department of Physics, University of Warwick, Gibbet Hill Road, Coventry CV4 7AL, United Kingdom*<sup>7</sup>*Diamond Light Source Ltd., Diamond House, Harwell Science and Innovation Campus, Didcot, Oxfordshire OX11 0DE, United Kingdom*<sup>8</sup>*Department of Chemistry, Princeton University, Princeton, New Jersey 08540, USA*

(Received 4 October 2016; revised manuscript received 5 January 2017; published 14 February 2017)

Surface x-ray diffraction has been used to determine the quantitative structure of the (101) termination of anatase TiO<sub>2</sub>. The atomic displacements from the bulk-terminated structure are significantly different from those previously calculated with density functional theory (DFT) methods with discrepancies for the Ti displacements in the [10 $\bar{1}$ ] direction of up to 0.3 Å. DFT calculations carried out as part of the current paper provide a much better agreement through improved accuracy and thicker slab models.

DOI: [10.1103/PhysRevB.95.075416](https://doi.org/10.1103/PhysRevB.95.075416)**I. INTRODUCTION**

The numerous technological applications in which the surfaces of titanium dioxide (TiO<sub>2</sub>) are important have motivated many studies of model single-crystal TiO<sub>2</sub> terminations [1]. Of particular interest is the elucidation of the geometric structure of the surface, which is essential for the mechanistic understanding of surface processes. This helps to improve existing uses of the material or establish new applications. To date, however, only the structures of the (110) and (011) surfaces of the rutile polymorph of TiO<sub>2</sub> have been determined quantitatively using diffraction methods [2,3]. No analogous work has previously been performed on the surfaces of anatase (a) TiO<sub>2</sub> due to the limited size and quality of available single-crystal samples. Improvements in instrument capability and sample quality now make it possible to perform the experimental measurement. In this article we provide a fully quantitative surface structural determination of a-TiO<sub>2</sub>(101) using surface x-ray diffraction (SXRD) and compare the results with density functional theory (DFT) calculations. The results will play a role in understanding the origin of the well-known higher photoactivity of anatase [4,5], which might be linked in some way to the surface structure.

The a-TiO<sub>2</sub>(101) surface is proposed to terminate in rows of two-coordinated oxygen and five-coordinated titanium atoms [6,7] along the [0 $\bar{1}$ 0] direction with an unreconstructed (1 × 1) termination forming a "sawtooth" structure (see Fig. 1). This is consistent with the unit-cell symmetry observed with

low-energy electron diffraction (LEED) [8] as well as with scanning tunneling microscopy (STM) images that evidence rows running along the [0 $\bar{1}$ 0] azimuth and terraces separated by 3.5-Å steps [9].

There have been a number of calculations of the a-TiO<sub>2</sub>(101) surface structure [10–13]. In general, there is good agreement between the atomic displacements predicted by these studies. Displacements in the [101] direction of the undercoordinated atoms in the top layer O(1) and Ti(1) in Fig. 1 relax towards the bulk. In contrast, fully coordinated atoms in the topmost layer [i.e., O(2), O(3), and Ti(2)] move away from the bulk, and subsurface oxygen atoms [O(4)] relax towards the bulk. Displacements of atoms in the next equivalent layer [O(5–8) and Ti(3,4)] shift in the same direction with respect to the bulk as their equivalents in the topmost layer but to a lower extent. With few exceptions [10,11], predictions of the displacements along the [10 $\bar{1}$ ] azimuth agree in the direction relative to the bulk lattice coordinates. Where they are reported, displacements along the [0 $\bar{1}$ 0] direction are negligible [11,12]. This behavior is to be expected given the maintenance of symmetry along the rows observed with STM [9,14].

In this paper we rigorously test the results of the structure calculations using SXRD. The experimental results differ from theoretical calculations in that a significant difference in both the magnitude and the direction of the displacements in the top few layers is observed, resulting in differences in the interlayer distances. This discrepancy is resolved by our new calculations, which employ a model containing a thicker slab and a more accurate basis set.

**II. EXPERIMENTAL AND COMPUTATIONAL DETAILS**

Experimental work was carried out at Diamond Light Source utilizing the facilities of the Surfaces and Interfaces Laboratory for sample preparation and beamline I07 for SXRD measurements [15]. Preparation of a (7 × 3 × 1)-mm natural

\*g.thornton@ucl.ac.uk

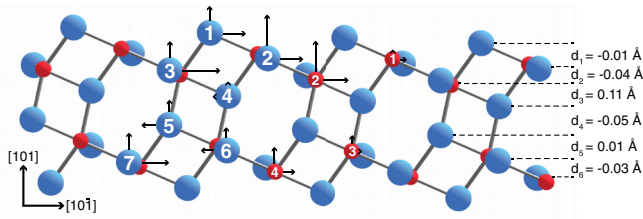


FIG. 1. Ball and stick representation of the UHV-prepared a-TiO<sub>2</sub>(101) surface. Substrate oxygen and titanium atoms are colored blue and red, respectively. The numerical labeling of the atoms/layers is employed in Tables I–III and V for identification purposes. Vertical and horizontal arrows represent the direction of atomic displacements of the best-fit solution derived from SXRD in the [101] and [101̄] directions, respectively. The length of the arrows is proportional to the relative magnitude. Also shown are the changes in interlayer distances  $d_{1-6}$  from their bulk positions.

a-TiO<sub>2</sub>(101) crystal (MaTecK) used repeated sputter-anneal cycles, consisting of Ar<sup>+</sup> bombardment ( $P \sim 10^{-5}$  mbar, 1 keV, 30 min) along with annealing to  $\sim 1000$  K in UHV for 10 min. Surface quality was monitored using LEED, x-ray photoelectron spectroscopy (XPS), and STM. The as-prepared a-TiO<sub>2</sub>(101) surface was free of contamination, although a small amount of argon was embedded during the preparation process (see Fig. 2). The surface also produced a sharp (1 × 1) LEED pattern identical to those previously observed [8,16], and STM images (see Fig. 3) evidence the presence of terraces [9,16] separated by 3.5 Å steps, corresponding to the separation between equivalent [101] planes.

After preparation, the same sample was transferred to a portable vacuum chamber ( $P \sim 1 \times 10^{-8}$  mbar), henceforth referred to as a "baby chamber," which incorporated a hemispherical beryllium window allowing transmission of x-rays to and from the sample surface within a UHV environment. To ensure that there was no significant reaction of the surface over the period of the SXRD measurement, we recorded STM images after exposing the surface to a residual vacuum of  $\sim 4 \times 10^{-8}$  mbar for 2 h. These reveal a clean surface with a small amount of randomly distributed hydroxyls [17] (see Fig. 4), which will not significantly affect the SXRD results. Moreover, modification of the surface over longer periods can be excluded on the basis of reference crystal truncation rod

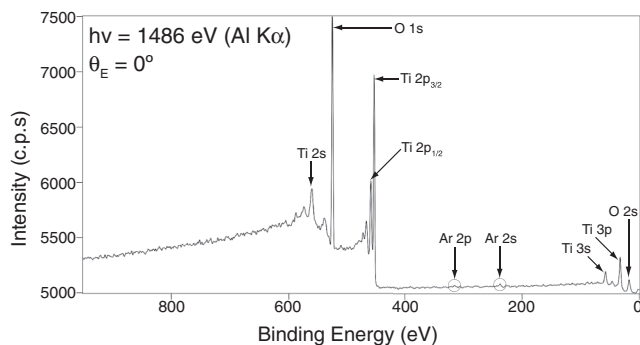


FIG. 2. Normal emission Al  $K\alpha$  XPS spectrum of the UHV-prepared anatase-TiO<sub>2</sub>(101) surface prior to the SXRD measurement.

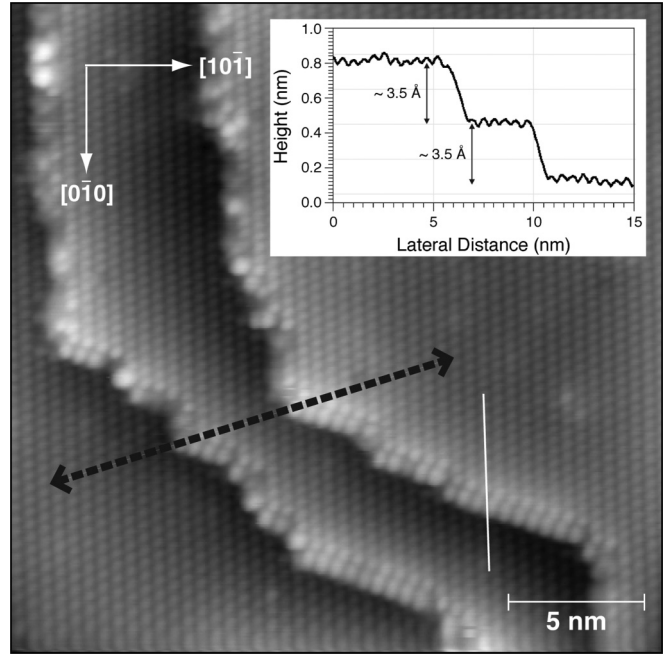


FIG. 3. STM image ( $23.6 \times 23.6$  nm<sup>2</sup>, constant current mode,  $V_{\text{sample}} = +1.2$  V,  $I_{\text{tunnel}} = 200$  pA) of the UHV-prepared anatase-TiO<sub>2</sub>(101) surface. The white line highlights the apparent phase difference of the rows in the [010] direction across a step edge. The line scan evidences 3.5 Å steps between terraces.

(CTR) measurements (see below). The baby chamber was mounted on a (2 + 3) circle diffractometer [18], located in the first experimental hutch on I07, with the sample surface in the horizontal plane. Data were acquired at room temperature with a photon energy of  $h\nu = 17.7$  keV ( $\lambda = 0.701$  Å) and an incidence angle of 1° using a combination of rocking curve [19] and stationary mode [20] data-acquisition techniques that employed a PILATUS 100K area pixel detector. An orthogonal unit cell defined by lattice vectors ( $\mathbf{a}_1, \mathbf{a}_2, \mathbf{a}_3$ ) was used to orient the crystal during the experimental data-acquisition procedure. The magnitudes of these lattice vectors are  $\mathbf{a}_1 = \sqrt{(a^2 + c^2)}$ ,  $\mathbf{a}_2 = b$ , and  $\mathbf{a}_3 = 3c\sqrt{[1 + (c^2/a^2)]}$ , where  $a = b = 3.7821$  and  $c = 9.5022$  Å are the lattice constants of the tetragonal anatase unit cell [21]. The reciprocal space that is derived from this lattice shows a set of permitted ( $h, k, l$ ) reflections satisfying the condition  $(h + k) = 2n$ .

Theoretical modeling of experimental structure factors employed the ROD analysis program [22]. A pseudo-orthorhombic surface cell with cell parameters of  $a' = 10.23$ ,  $b' = 3.71$ ,

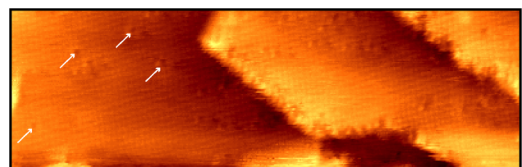


FIG. 4. STM image ( $30 \times 9.4$  nm<sup>2</sup>,  $V_{\text{sample}} = +1.2$  V,  $I_{\text{tunnel}} = 100$  pA) of the UHV-prepared anatase-TiO<sub>2</sub>(101) surface after exposure to a residual vacuum of  $\sim 4 \times 10^{-8}$  mbar for 2 h. The white arrows indicate the presence of hydroxyls on the surface.

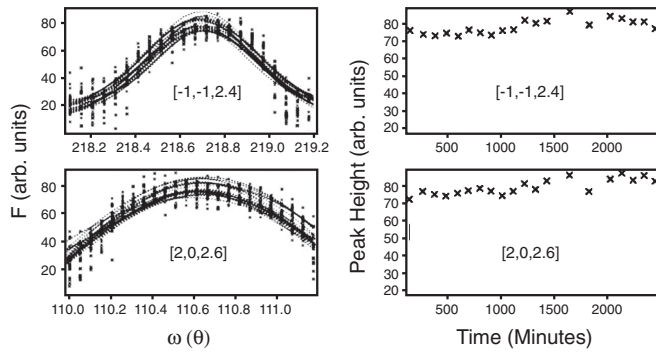


FIG. 5. (Left) Reference rocking curve intensities (crosses) and fit (dashed lines) recorded throughout the SXRD measurement. (Right) The corresponding rocking curve fit peak height variation with the time of the CTRs from the a-TiO<sub>2</sub>(101) surface.

$c' = 24.60 \text{ \AA}$ ,  $\alpha = \gamma = 90^\circ$ , and  $\beta = 88.98^\circ$  was used to model the surface structure as opposed to the orthogonal cell used during experimental data acquisition. This was in order to align the  $c$  axis with the surface normal direction of the orthogonal cell for a more efficient calculation of displacements in the [101] direction. This pseudo-orthorhombic cell is more closely commensurate to the tetragonal cell than the orthogonal alignment cell. The measured  $L$  indices were recalculated according to this new ( $a', b', c'$ ) cell.

DFT calculations were performed using the Perdew-Burke-Ernzerhof (PBE) functional within a plane-wave pseudopotential scheme. We used ultrasoft pseudopotentials with a kinetic-energy cutoff of 35 (350) Ry for the smooth part of the electronic wave functions (augmented electron density). The surface was modeled using a  $(3 \times 1)$  slab of ten Ti layers with a total of 180 atoms per unit cell. The vacuum region between adjacent slabs was  $15 \text{ \AA}$  wide. Theoretical lattice parameters determined with the same setup were employed.  $k$  space was sampled using a  $(2 \times 2 \times 1)$  Monkhorst-Pack mesh; test calculations showed essentially no difference when using a denser  $(4 \times 4 \times 1)$  mesh. All atoms in the slab were fully relaxed except the Ti atoms in the bottom layer, which were kept fixed at their bulk positions; relaxation was carried out until residual forces were less than  $0.03 \text{ eV/\AA}$ .

### III. RESULTS AND DISCUSSION

An extensive dataset of 15 CTRs totaling 2401 structure factors was acquired from the a-TiO<sub>2</sub>(101) surface. The complete dataset for this surface was recorded in  $\sim 15$  h. Subsequently they were reduced and corrected to produce plots of structure factor against perpendicular momentum transfer, henceforth referred to as CTR(s). Additionally, rocking scans at specific ( $hkl$ ) anti-Bragg position(s) of the CTRs were repeated regularly to monitor changes in diffracted intensity caused by sample degradation or beam damage throughout the lifetime of the experiment. The intensity of these reference

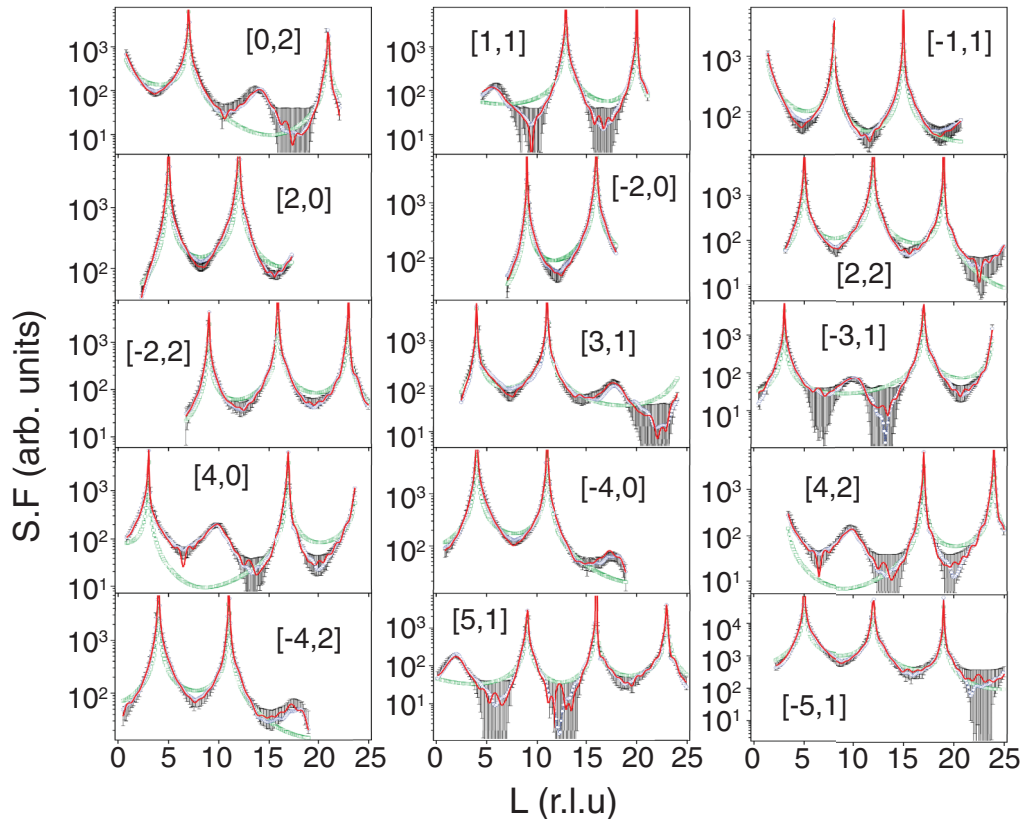


FIG. 6. Experimental (error bars) and best-fit calculated CTRs of the UHV-prepared anatase-TiO<sub>2</sub>(101) surface using the bulk-terminated (green squares),  $\beta$ -roughness (blue circles), and terraced-roughness models (red line).

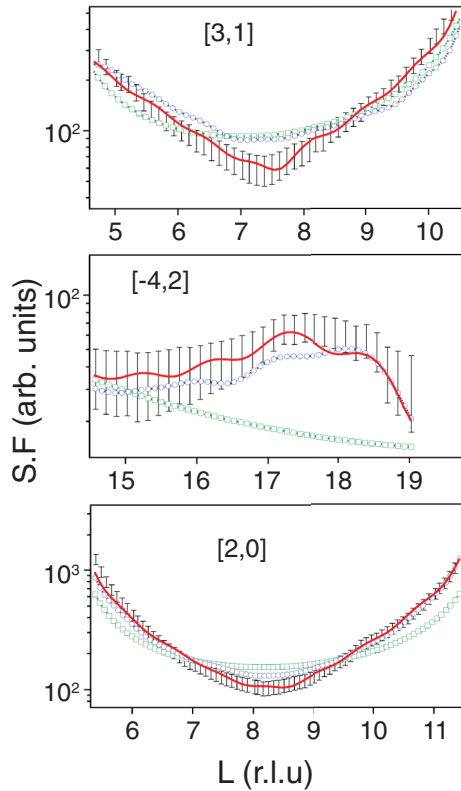


FIG. 7. A comparison of anti-Bragg regions for three selected experimental (error bars) and best-fit calculated CTRs from the clean UHV-prepared anatase-TiO<sub>2</sub>(101) surface using the bulk terminated (green squares),  $\beta$ -roughness (blue circles), and terraced-roughness models (red line).

scans remained essentially constant throughout measurement of the surface as shown in Fig. 5.

Assessment of goodness of fit between the experimental and the theoretical structure factors was achieved quantitatively using the normalized  $\chi^2$  [23] and  $R$  factor [24]. A systematic approach was adopted for structure determination

whereby a bulk-terminated model initially was tested, and then atoms were allowed to relax until satisfactory agreement was achieved. A comparison of the experimental CTRs with those modeled are shown in Fig. 6 with an enlarged part of three CTRs shown in Fig. 7. The bulk-terminated model gave a  $\chi^2$  of 9.32 and a  $R$  value of 0.42, see Figs. 6 and 7 (green squares). It is clear that a structure with the surface atoms at the bulk lattice positions does not account for the experimentally observed anti-Bragg modulations. Refinement of the atomic coordinates (94 parameters), Debye-Waller (DW) factors (19 parameters), site occupancies (one parameter), and  $\beta$ -roughness parameter in this structure achieved a minimum  $\chi^2$  of 1.43 and a  $R$  value of 0.17. However the " $\beta$ -approximated" roughness calculation [25] typically used within ROD was found to be less than ideal for structural refinement of the a-TiO<sub>2</sub>(101) surface. This is due to a surface roughness arising from the highly stepped nature of the surface.

In the  $\beta$ -roughness approximation, roughness is simulated by having fractionally occupied layers, which sit atop the topmost fully occupied layer with the occupation decreasing exponentially away from the bulk. As a result, the  $\beta$ -roughness model does not completely reproduce the anti-Bragg modulations in the experimental data as shown in Figs. 6 and 7 (blue circles). Introduction of a terraced-roughness approximation as used by Magdans *et al.* [26] allows the step-related surface roughness to be better simulated. Two coherently scattering domains with identical terminations (i.e., atomic displacement from bulk coordinates and DW factors) were used, the only difference between the domains being the relative height from the bulk at which the termination(s) occurs as shown in Fig. 8. This model also takes into account the apparent phase difference, observed with STM, of the rows in the [0 $\bar{1}$ 0] direction across a step edge (see Fig. 3). The degree of roughness (relative area) is manipulated using the occupancy of the lower termination  $m$  with a permitted range of  $0 \leq m \leq 0.5$  allowed during structure refinement. Use of the terraced-roughness model during structure determination resulted in a  $\chi^2$  of 1.02 and a  $R$  value of 0.14, the CTRs from which are shown in Figs. 6 and 7 (red line). In the best-fit structure  $m = 0.26$ ,

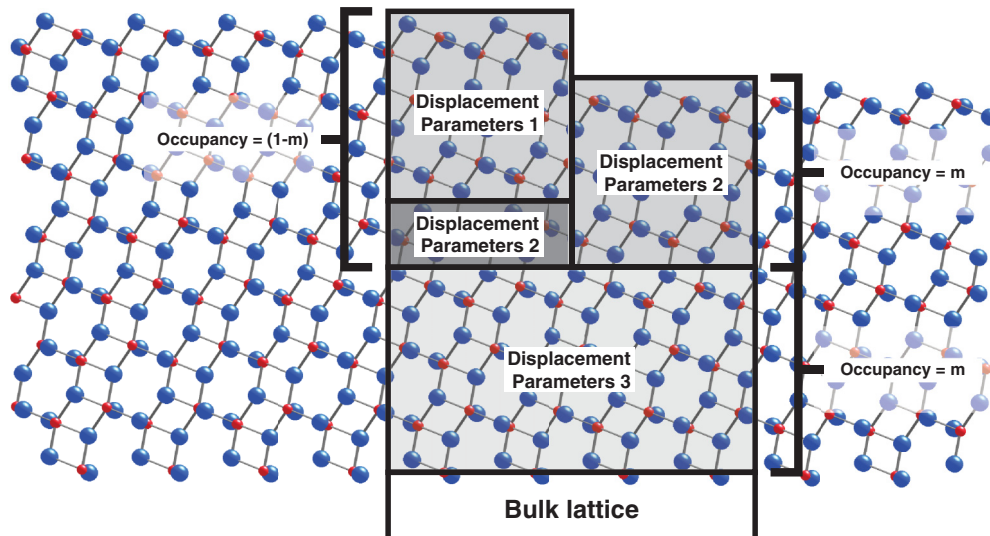


FIG. 8. Illustration of the terraced-roughness approximation used for structure determination of the UHV-prepared a-TiO<sub>2</sub>(101) surface.

TABLE I. Comparison of atomic displacements, given in angstroms, away from bulk-terminated a-TiO<sub>2</sub>(101)(1 × 1). Experimental SXRD results are compared with new DFT calculations as well as with previously published DFT calculations [10,12,13]. The greatest discrepancies between SXRD and DFT are highlighted in either bold (displacement in different direction) or underlined (difference > 0.1 Å). See Fig. 1 for a key to the identity of the atoms.

Atom	SXRD (This paper)		DFT		(PBE)		(PBE0)		Perdew-Wang Functional (PW1PW)	
	$(\chi^2 = 1.02)$		(this paper)		DFT [10]		DFT [13]		DFT [12]	
	$\Delta[10\bar{1}]Å$	$\Delta[101]Å$	$\Delta[10\bar{1}]Å$	$\Delta[101]Å$	$\Delta[10\bar{1}]Å$	$\Delta[101]Å$	$\Delta[10\bar{1}]Å$	$\Delta[101]Å$	$\Delta[10\bar{1}]Å$	$\Delta[101]Å$
O(1)	0.11 ± 0.02	0.07 ± 0.01	0.17	0.14	<u>0.29</u>	<b>-0.02</b>	0.41	<b>-0.03</b>	<u>0.35</u>	<b>-0.02</b>
Ti(1)	0.03 ± 0.01	0.01 ± 0.01	0.04	0.01	<u>0.02</u>	<b>-0.18</b>	<u>0.15</u>	<b>-0.19</b>	0.09	<b>-0.16</b>
O(2)	0.11 ± 0.01	0.15 ± 0.01	0.12	<u>0.33</u>	0.16	0.19	<u>0.28</u>	0.18	<u>0.24</u>	0.21
O(3)	0.18 ± 0.01	0.08 ± 0.01	0.09	0.16	0.17	0.06	0.28	0.06	0.22	0.05
Ti(2)	0.12 ± 0.01	0.15 ± 0.01	0.07	<u>0.28</u>	0.17	0.20	<u>0.30</u>	0.18	<u>0.23</u>	0.18
O(4)	-0.01 ± 0.02	0.01 ± 0.01	<b>0.07</b>	0.07	<b>0.15</b>	<b>-0.07</b>	<b>0.26</b>	<b>-0.08</b>	<b>0.22</b>	<b>-0.06</b>
O(5)	-0.07 ± 0.01	0.06 ± 0.01	<b>0.02</b>	0.13	<b>0.06</b>	0.04	<b>0.17</b>	0.03	<b>0.13</b>	0.03
Ti(3)	0.01 ± 0.01	0.04 ± 0.01	<b>-0.09</b>	0.02	<b>-0.04</b>	<b>-0.14</b>	0.07	<b>-0.12</b>	0.04	<b>-0.10</b>
O(6)	-0.06 ± 0.01	0.05 ± 0.01	-0.03	0.09	-0.02	<b>-0.04</b>	<b>0.09</b>	<b>-0.05</b>	<b>0.07</b>	<b>-0.02</b>
O(7)	0.13 ± 0.01	0.08 ± 0.01	<b>-0.02</b>	0.10			0.13	0.03	0.10	0.01
Ti(4)	0.06 ± 0.01	0.08 ± 0.01	<b>-0.02</b>	0.16			0.13	0.09	0.10	0.08

in other words, there is a 3:1 ratio of the two domains. The feasibility of introducing a third terrace of occupancy  $n$  was investigated to simulate a greater severity of roughness, but this achieved no appreciable improvement in the  $\chi^2$  and was not pursued further. Independent atomic occupancies of inequivalent sites within the structure also were investigated during early fitting, however full occupancy of all sites (i.e., no vacancies) was preferred. As for the DW factors, these all adopted reasonable values where the highest corresponds to the topmost surface layer ( $O = 4.4 \pm 0.1, Ti = 1.9 \pm 0.1 \text{ \AA}^2$ ) and progressively decreasing to the lowest value, that is, the bulk DW factors ( $O = 0.4 \pm 0.1, Ti = 0.6 \pm 0.1 \text{ \AA}^2$ ), which also were refined. The surface fraction parameter indicates that the entire surface adopted the geometry described by the best-fit model.

TABLE II. SXRD-derived optimized locations of atoms, given in angstroms, for the best-fit terrace roughness model. Also listed are the atomic positions for the bulk truncated coordinates for a-TiO<sub>2</sub>(101)(1 × 1). See Fig. 1 for a key to the identity of the atoms.

Atom	(1 × 1) bulk-terminated coordinates (Å)		Optimized positions (Å)	
	$\Delta[10\bar{1}]Å$	$\Delta[101]Å$	$\Delta[10\bar{1}]Å$	$\Delta[101]Å$
O(1)	4.75	22.70	4.86	22.77
Ti(1)	6.57	21.97	6.60	21.97
O(2)	6.94	21.82	7.05	21.97
O(3)	3.28	21.23	3.47	21.31
Ti(2)	3.65	21.09	3.77	21.24
O(4)	5.48	20.36	5.47	20.36
O(5)	3.29	19.18	3.22	19.24
Ti(3)	5.11	18.45	5.12	18.49
O(6)	5.48	18.30	5.42	18.35
O(7)	1.82	17.72	1.96	17.80
Ti(4)	2.19	17.57	2.25	17.65

Table I lists the atomic displacements for our SXRD optimum structure (atomic coordinates given in Table II) as well as those obtained in previous theoretical calculations [10,12,13]. A comparison of the experimental and theoretical results reveals the lack of quantitative agreement between the two. Disparities in the displacements are present for most atoms in the top three layers. With the exception of a few, these discrepancies are limited to a difference in the magnitude of the displacement (underlined if >0.1 Å) and the direction (highlighted in bold). As a result, there are significant differences observed in the magnitude of the interlayer distances throughout the selvedge (Table III). Our experimental results reveal a much-reduced change from bulk interlayer distances when compared to that of previous theoretical calculations. To establish the significance of these discrepancies, in particular, the very large discrepancies of the displacements in the [101] direction of Ti(1) and Ti(3), fitting to the models proposed by Lazzeri *et al.* [10], Labat *et al.* [13], and Esch *et al.* [12] was performed. This was carried

TABLE III. A comparison of the interlayer distances, given in angstroms, for the a-TiO<sub>2</sub>(101) surface. Experimental SXRD results are compared with new DFT calculations as well as with previously published DFT calculations. All interlayer distances for the theoretical models were extracted using fixed displacements on the best-fit terraced-roughness model derived from SXRD. The interlayer labels correspond with those seen in Fig. 1.

Interlayer	SXRD	DFT	(PBE)	(PBE0)	(PW1PW)
	(this paper)	(this paper)	DFT [10]	DFT [13]	DFT [12]
$d_1$	-0.01	-0.03	-0.02	-0.02	-0.04
$d_2$	-0.04	-0.05	-0.12	-0.12	-0.09
$d_3$	0.11	0.15	0.20	0.20	0.17
$d_4$	-0.05	-0.06	-0.11	-0.11	-0.09
$d_5$	0.01	0.07	0.11	0.13	0.09
$d_6$	-0.03	-0.07	-0.15		-0.11

TABLE IV. A  $\chi^2/R$ -factor comparison of surface models attempted during iterative fitting process for the a-TiO<sub>2</sub>(101) surface. All theoretical models were tested on the best-fit terraced-roughness model derived from SXRD.

Model	$\chi^2$	$R$
Bulk terminated	9.32	0.42
$\beta$ roughness	1.43	0.17
Labat DFT $\pm 0.1$ Å	1.62	0.19
Lazzeri DFT $\pm 0.1$ Å	1.63	0.19
Esch DFT $\pm 0.1$ Å	1.37	0.18
Terraced roughness	1.02	0.14

out using the terraced-roughness model with displacement constraints of  $\pm 0.1$  Å from the starting value to ensure that the optimized structure derived from SXRD was not the result of a local minimum. However, the  $\chi^2$  and  $R$  values were significantly worse when fitting to previously published structures as summarized in Table IV. When the displacement constraints of the atoms were removed after initial fitting of the DFT structures, the displacements rapidly converged towards the displacements of the optimized SXRD structure and a decrease in the  $\chi^2$  and  $R$  values was observed. This effect was most pronounced in atoms Ti(1) and Ti(3). A list of the Ti-O bond lengths of the optimized a-TiO<sub>2</sub>(101) surface is given in Table V.

In contrast to the computational results previously published, the theoretically predicted geometry from this paper corresponds rather well with that derived from SXRD; the large discrepancies observed in the displacements of Ti(1) and Ti(3) in the [101] direction have now significantly reduced, and only the displacements of O(2) and Ti(2) in the [101] direction displace with magnitudes greater than 0.1 Å.

TABLE V. Titanium oxygen bond lengths in the SXRD structure of the a-TiO<sub>2</sub>(101) surface.

Bond	Bond length (Å)	Bond	Bond length (Å)
Ti(1)-O(1)	1.90 $\pm$ 0.02	Ti(2)-O(5)	2.08 $\pm$ 0.01
Ti(1)-O(2)	1.94 $\pm$ 0.01	Ti(3)-O(4)	1.91 $\pm$ 0.01
Ti(1)-O(3)	2.07 $\pm$ 0.01	Ti(3)-O(5)	2.03 $\pm$ 0.01
Ti(1)-O(4)	1.99 $\pm$ 0.02	Ti(3)-O(6)	1.92 $\pm$ 0.01
Ti(2)-O(1)	1.89 $\pm$ 0.01	Ti(3)-O(7)	2.06 $\pm$ 0.01
Ti(2)-O(2)	1.97 $\pm$ 0.01	Ti(4)-O(5)	1.89 $\pm$ 0.01
Ti(2)-O(3)	1.92 $\pm$ 0.01	Ti(4)-O(6)	2.05 $\pm$ 0.01
Ti(2)-O(4)	1.89 $\pm$ 0.02	Ti(4)-O(7)	1.89 $\pm$ 0.01

#### IV. SUMMARY

SXRD has been used to experimentally determine the quantitative geometric structure of a-TiO<sub>2</sub>(101). There are notable disagreements between the experimental results and previous calculations, in particular, the two topmost atoms O(1) and Ti(1) are found experimentally to move away from the bulk. The results of DFT calculations in this paper are more consistent with the experimentally derived geometric structure. This structure determination will support future work in achieving a greater understanding of surface processes, for instance, the photocatalytic activity of a-TiO<sub>2</sub>.

#### ACKNOWLEDGMENTS

This work was funded by an ERC Advanced Grant ENERGYSURF (G.T.), EPSRC (U.K.) (Grant No. EP/G067384/1), EU COST action CM1104, the Royal Society through a Wolfson Merit Award, MINECO (Spain) through Project No. MAT2015-68760-C2-2-P. J.P.W.T. acknowledges support from the Diamond Light Source.

- 
- [1] C. L. Pang, R. Lindsay, and G. Thornton, *Chem. Rev.* **113**, 3887 (2013).
- [2] G. Cabailh, X. Torrelles, R. Lindsay, O. Bikondoa, I. Joumar, J. Zegenhagen, and G. Thornton, *Phys. Rev. B* **75**, 241403(R) (2007).
- [3] X. Torrelles, G. Cabailh, R. Lindsay, O. Bikondoa, J. Roy, J. Zegenhagen, G. Teobaldi, W. A. Hofer, and G. Thornton, *Phys. Rev. Lett.* **101**, 185501 (2008).
- [4] T. Luttrell, S. Halpegamage, J. Tao, A. Kramer, E. Sutter, and M. Batzill, *Sci. Rep.* **4**, 4043 (2014).
- [5] J. Zhang, P. Zhou, J. Liu, and J. Yu, *Phys. Chem. Chem. Phys.* **16**, 20382 (2014).
- [6] P. M. Oliver, G. W. Watson, E. T. Kelsey, and S. C. Parker, *J. Mater. Chem.* **7**, 563 (1997).
- [7] A. Vittadini, A. Selloni, F. P. Rotzinger, and M. Grätzel, *Phys. Rev. Lett.* **81**, 2954 (1998).
- [8] R. Hengerer, B. Bolliger, M. Erbudak, and M. Grätzel, *Surf. Sci.* **460**, 162 (2000).
- [9] W. Hebenstreit, N. Ruzycski, G. S. Herman, Y. Gao, and U. Diebold, *Phys. Rev. B* **62**, R16334(R) (2000).
- [10] M. Lazzeri, A. Vittadini, and A. Selloni, *Phys. Rev. B* **63**, 155409 (2001).
- [11] X. G. Ma, C. Q. Tang, J. Q. Huang, L. F. Hu, X. Xue, and W. B. Zhou, *Acta Phys. Sinica* **55**, 4208 (2006).
- [12] T. R. Esch, I. Gadaczek, and T. Bredow, *Appl. Surf. Sci.* **288**, 275 (2014).
- [13] F. Labat, P. Baranek, and C. Adamo, *J. Chem. Theory Comput.* **4**, 341 (2008).
- [14] Y. He, O. Dulub, H. Cheng, A. Selloni, and U. Diebold, *Phys. Rev. Lett.* **102**, 106105 (2009).
- [15] C. Nicklin, T. Arnold, J. Rawle, and A. Warne, *J. Synchrotron Radiat.* **23**, 1245 (2016).
- [16] O. Dulub and U. Diebold, *J. Phys.: Condens. Matter* **22**, 84014 (2010).
- [17] O. Stetsovych, M. Todorović, T. K. Shimizu, C. Moreno, J. W. Ryan, C. P. León, K. Sagisaka, E. Palomares, V. Matolín, D. Fujita, R. Perez, and O. Custance, *Nat. Commun.* **6**, 7265 (2015).
- [18] E. Vlieg, *J. Appl. Crystallogr.* **31**, 198 (1998).
- [19] I. K. Robinson, *Aust. J. Phys.* **41**, 359 (1988).

- [20] X. Torrelles and J. Rius, *J. Appl. Crystallogr.* **37**, 395 (2004).
- [21] J. K. Burdett, T. Hughbanks, G. J. Miller, J. W. Richardson, and J. V. Smith, *J. Am. Chem. Soc.* **109**, 3639 (1987).
- [22] E. Vlieg, *J. Appl. Crystallogr.* **33**, 401 (2000).
- [23] R. Feidenhans'l, *Surf. Sci. Rep.* **10**, 105 (1989).
- [24] G. H. Stout and L. H. Jensen, *X-Ray Structure Determination: A Practical Guide* (Macmillan, New York, 1968).
- [25] I. K. Robinson, *Phys. Rev. B* **33**, 3830 (1986).
- [26] U. Magdars, H. Gies, X. Torrelles, and J. Rius, *Eur. J. Mineral.* **18**, 83 (2006).